JOURNAL OF SOLID STATE CHEMISTRY **138,** 18–31 (1998)
ARTICLE NO. SC977728

Ordered K_2NiF_4 Structure of the Solids $La_2Li_{1/2}M_{1/2}O_4$ (M(III) = Co, Ni, Cu) and the Bonding Properties of the MO_6 Polyhedra in Various Compounds of This Type

Salam Abou-Warda, Walter Pietzuch, Gerd Berghöfer, Ute Kesper, Werner Massa, and Dirk Reinen

Fachbereich Chemie und Zentrum für Materialwissenschaften der Philipps-Universität, Hans-Meerwein-Strasse, D-35043 Marburg, Germany

Received July 10, 1997; in revised form December 1, 1997; accepted December 2, 1997

From single-crystal X-ray analyses it is derived that the compounds $La_2Li_{1/2}M_{1/2}O_4$ (M(III) = Co, Ni, Cu) crystallize in an orthorhombic variant of the K_2NiF_4 structure, with an ordered distribution of the Li(I) and M(III) cations on the octahedral sites. Accordingly, the unit cell is enlarged perpendicular to the [001] direction (space group *Ammm*, No. 65), though the metric remains tetragonal. The average M–O bond distances indicate low-spin configurations for the three $3d^n$ cations, which is supported by spectroscopic measurements and ligand field considerations. The MO_6 and LiO_6 polyhedra are distinctly tetragonally elongated due to host site strains but superimposed by strong additional distortion components in the case of NiO_6 and CuO_6 as a consequence of vibronic Jahn–Teller coupling. Reported compounds of the same composition with M(III) = Al, Ga, and Mn seem to adopt the same structure. In contrast to the copper(III) compound, $La_2Li_{1/2}Au_{1/2}O_4$ crystallizes in the structurally related ordered Nd_2CuO_4-type lattice with square-planar AuO_4 entities. © 1998 Academic Press

I. INTRODUCTION

The K_2NiF_4 structure is known from the pioneering work of Balz and Plieth (1). K_2NiF_4-type $La_2Li_{1/2}M_{1/2}O_4$ (M = Co, Ni, Cu) solids were first described by Blasse (2) and later characterized by Demazeau and coworkers, who also reported the spectroscopic and magnetic properties of these compounds (3–6). It is the purpose of the current study to extend these investigations, which were performed exclusively on powder materials, by single-crystal X-ray analysis. The recent interest in the solid state physics of the high-valence states of nickel and copper in oxide ceramics has stimulated this work. Of particular importance here is whether a cation order between Li(I) and the transition metal ion exists, because the local MO_6 bonding properties critically depend on this structural feature. Such an order, which, to our knowledge, has not been observed in this structure type so far, is very difficult to deduce from X-ray powder diagrams.

It is further remarkable that one can stabilize cobalt, nickel, and, in particular, copper in the +III oxidation state in this specific oxide matrix, which is not easy otherwise. It is even possible to generate Co(IV) in the high-pressure phase $Sr_{1/2}La_{3/2}Li_{1/2}Co_{1/2}O_4$ (7, 8). We have prepared $La_{2-x}Sr_xLi_{1/2}Co_{1/2}O_4$ ($0 \le x < 0.3$) mixed crystals, and a single-crystal X-ray study has been performed. Furthermore, a structural investigation of $La_2Li_{1/2}Au_{1/2}O_4$ is in progress (9).

The bonding properties of the MO_6 polyhedra in these compounds are analyzed in greater detail by means of spectroscopic methods and by comparison with spectroscopic data available for the M(III) cations in fluoridic ligand fields and for cations such as Cr(III) and Mn(III) in various oxidic solids. More recently reported oxide ceramics of the same composition with M(III) = Al (10), Ga (11), and Mn (12) are included in the discussion.

II. EXPERIMENTAL

Synthesis

Mixtures of $La(OH)_3$, Li_2CO_3, and Co_3O_4 or $NiCO_3$ or CuO were carefully homogenized by mortaring and heated in a corundum boat at 800°C in flowing oxygen for 12–15 h. Li_2CO_3 was chosen because of its low melting point (723°C) and its corresponding high reactivity. It was applied in about 50% excess to compensate the loss by evaporation at the chosen sintering temperature. The mortared product was heated with water to remove most of the excess Li_2CO_3. The very stable $La_2Li_{1/2}M_{1/2}O_4$ solids obtained are brown, brown grayish, and red for M = Co, Ni, and Cu, respectively. A successive treatment in a Soxhlet extractor for about 8 h using H_2O as the solvent is necessary, however, to obtain the pure reaction compounds without an admixture of Li_2CO_3. The latter is indicated particularly by the peaks at 1435, $\cong$1495, and $\approx 3465\,cm^{-1}$ in the IR spectra (Fig. 1).

The average oxidation states were determined from powder materials, which were largely pure, by iodometric

0022-4596/98 $25.00

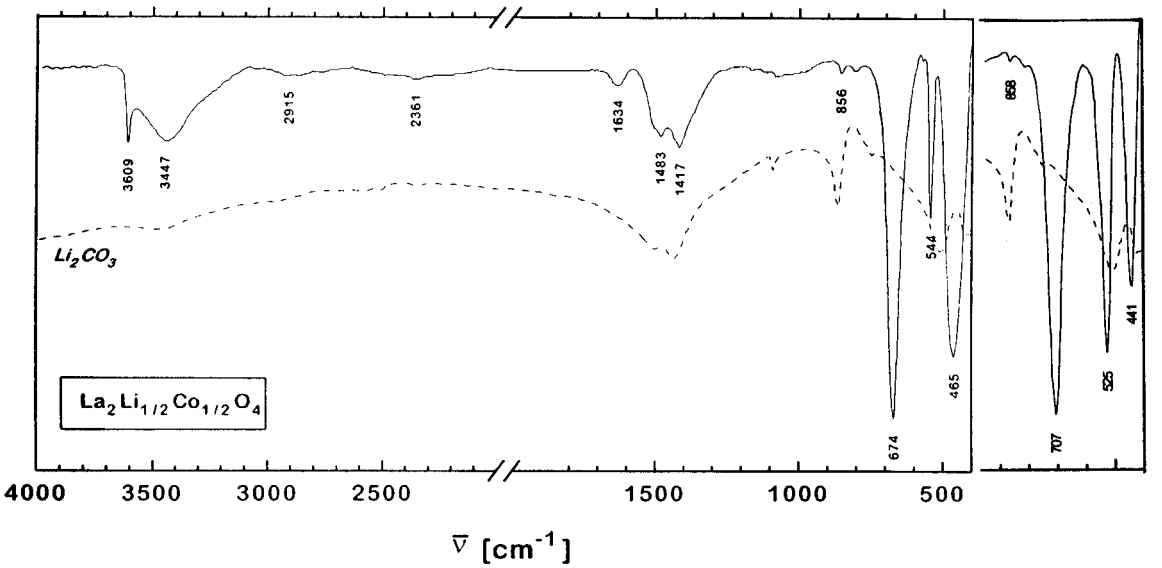

FIG. 1. IR spectrum of a $La_2Li_{1/2}Co_{1/2}O_4$ powder sample in the region between 400 and 4000 cm^{-1}. The spectrum of Li_2CO_3 is also shown. The broad absorption at about 2900 cm^{-1} is due to Nujol. The IR absorptions in the region 400–1000 cm^{-1} are additionally depicted for $La_2Li_{1/2}Cu_{1/2}O_4$.

titration. They were larger than +III by 0.1_5 and 0.1 for cobalt and nickel, respectively, and exactly +III in the case of copper. Analytical data (AAS) for Cu and Li (percentage by weight) in the copper solid (calculated values in parentheses) are 8.55 (8.43) and 0.97 (0.92). Whereas the molar Li/M ratio is close to one for M = Cu, as expected, it is smaller in the cases of M = Ni and, in particular, M = Co. The cited results indicate the presence of Co(IV) and Ni(IV), the charge compensation occurring most probably by vacancies in the Li(I) sublattice. We refrain from giving further analytical data, because they are mostly obscured by admixed Li_2CO_3.

Single crystals of the title compounds were obtained from a LiOH melt containing La_2O_3 and Co_3O_4 (or CuO or NiO) in stoichiometric amounts. The mixture was heated to 800°C and left at this temperature until most of the excess LiOH was evaporated. After cooling, the solidified melt was treated with boiling water for about 4–8 h, leaving rather small single crystals as the residue. The cobalt and nickel compounds were thin rectangular plates, whereas the habitus of the copper compound was of needle-like appearance. The pycnometric and calculated densities of $La_2Li_{1/2}Ni_{1/2}O_4$ are 6.82 and 6.84 g/cm^3, respectively.

In our experience a preparation method using alkaline $LiOH/Li_2CO_3$ melts is more efficient than a synthesis based on the metal nitrates (4, 5), because it stabilizes the higher oxidation states of the $3d^n$ cations.

DTA investigations gave no indication for a phase transition between 20 and 1200°C.

Spectroscopic and Magnetic Investigations

UV–vis spectra in the region between 4000 and 28,000 cm^{-1} were recorded using the powder reflection technique. EPR measurements were performed at X- and Q-band frequencies in the temperature range between 300 and 4 K using a Bruker spectrometer. IR spectra were measured in transmission with a Bruker IFS 88 spectrometer.

Magnetic measurements were carried out with a SQUID magnetometer (Quantum Design, Model MPMS-5) in the temperature range 1.8–300 K and external fields up to 5.5 T.

X-Ray Diffraction Analysis

X-ray investigations were performed on powders with a Huber Guinier camera (Cu$K\alpha_1$ radiation, SiO_2 monochromator) or a Siemens D500 diffractometer (Cu$K\alpha$ radiation, secondary monochromator) and on single crystals using a precession camera (Enraf-Nonius, Mo$K\alpha$ radiation) and four-circle diffractometers (Mo$K\alpha$ radiation, graphite monochromator). For a doubtless distinction of weak superstructure reflections from possible "$\lambda/2$" effects arising from strong $2h2k2l$ reflections, the $\lambda/2$ ratio $f_{\lambda/2}$ of the Mo$K\alpha$ radiation used was determined experimentally at a test crystal and was found to be 0.0041. Thus, for strong $2h2k2l$ reflections the intensities of the corresponding hkl reflections were diminished by $f_{\lambda/2}I_{2h2k2l}$ (13). More experimental details are given in Table 1 and in the text.

TABLE 1
Unit Cell Parameters (pm) from Calibrated Powder Diffraction Data and Number of Observed Superstructure Reflections (n) of Compounds $La_2Li_{1/2}M_{1/2}O_4$

M	a	c	c/a	n
Co	534.73(2)	1261.1(1)	2.358	7
Ni	530.97(2)	1288.9(1)	2.427	9
Cu	526.80(2)	1318.8(1)	2.503	1

Crystal Structure of $La_2Li_{1/2}Ni_{1/2}O_4$

Very weak superstructure reflections are observed in the powder diffractogram (Fig. 2) and on the Guinier films with intensities $<1\%$ of those of the main reflections characteristic for the tetragonal K_2NiF_4 type. They are indexable with an enlarged unit cell according to $a' = a\sqrt{2}$, $c' = c$. If the structure of the K_2NiF_4 aristotype (space group (SG) $I4/mmm$) is described in an enlarged unit cell ($\mathbf{a}' = \mathbf{a} + \mathbf{b}$, $\mathbf{b}' = -\mathbf{a} + \mathbf{b}$, $\mathbf{c}' = \mathbf{c}$, SG $F4/mmm$), the Ni position splits into two sites. An ordered occupation of these with Li(I) and Ni(III) according to Fig. 3 leads to a symmetry reduction to the maximal orthorhombic subgroup $Ammm$, which accounts for the observed superstructure reflections. For the sake of keeping the relation to the K_2NiF_4 type, no transformation to the conventional $Cmmm$ setting is made. To confirm the space group and to reveal the structural details, two platelike single crystals were investigated. Both showed weak superstructure reflections in the a^*b^* plane leading to the aforementioned larger cell ($a' = a\sqrt{2}$). The additional reflections are compatible with either the extinction rule hkl, $k + l \neq 2n$ (A centering), or the extinction rule hkl, $h + k \neq 2n$ (B centering), which can be explained by the presence of domains of an ordered $Ammm$ structure in two orientations corresponding to a partially pseudomerohedral twinning, the twin plane being (110). The second domain type can be described in SG $Bmmm$ when related to the axes of the first $Ammm$ domain type. In the following we will call them A and B domains, respectively. Though the SG symmetry is orthorhombic, the metric of the unit cell remains tetragonal, causing the main reflections of both domains (hkl: $h + k$, $h + l = 2n$) to coincide. Different intensities for the A-superstructure and B-superstructure reflections indicate different volumes of A and B domains.

In addition to this twinning, the second crystal showed very weak diffuse streaks along the c^* direction with maxima at half a reciprocal translation, indicating stacking disorder of the planes along the c axis. For the data collection on a four-circle diffractometer, the first single crystal was used with no diffuse scattering. The crystal data and experimental conditions are given in Table 2.

The appearance of sharp A- and B-superstructure reflections gives evidence for the presence of large twin domains,

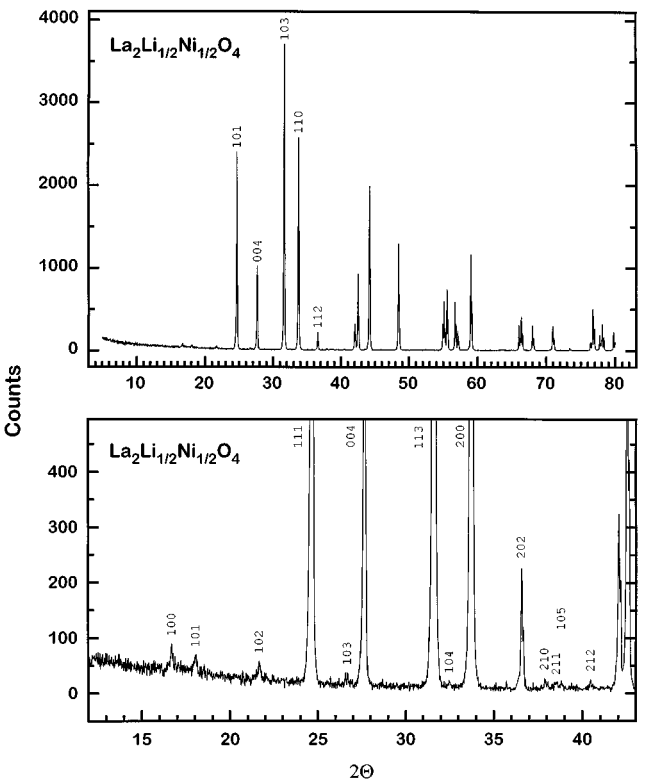

FIG. 2. X-ray powder diffraction pattern of $La_2Li_{1/2}Ni_{1/2}O_4$. The superstructure reflections are indicated in the diagram with the larger intensity scale below and refer to the enlarged orthorhombic cell, while the notations in the top figure are those of a K_2NiF_4-type structure.

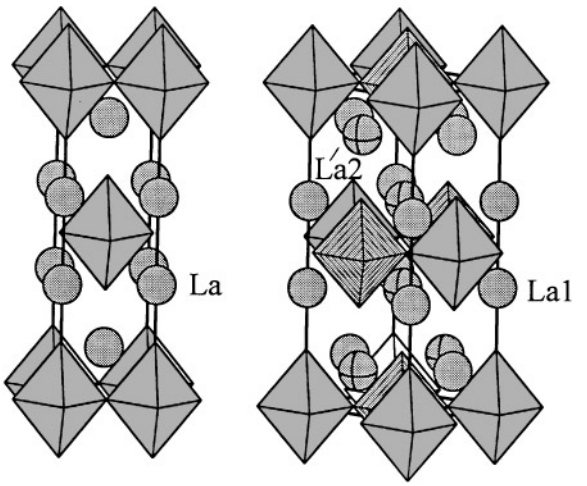

FIG. 3. (Left) K_2NiF_4-type unit cell of La_2NiO_4 (space group $I4/mmm$, No. 139) and (right) the superstructure induced by cation ordering in solids $La_2Li_{1/2}M_{1/2}O_4$ (space group $Ammm$, No. 65, shifted by $\delta x = \frac{1}{2}$ with respect to the atomic positions in Table 3). Lighter and darker shaded polyhedra are occupied predominantly by Li and M, respectively.

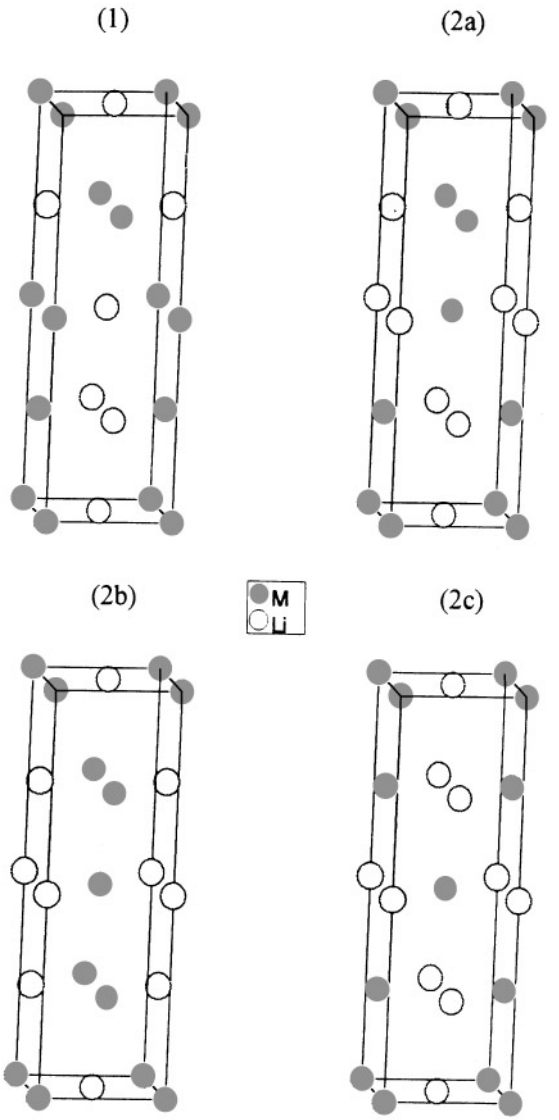

FIG. 4. Stacking order models with $c' = 2c$, displaying P-type (1) and I-type (2a–c) unit cells. The former readily explains the observed crystal twinning of solids $La_2Li_{1/2}M_{1/2}O_4$, the (001) plane at $c'/2$ being the twinning interface between an A and B cell.

larger than the coherence lengths of the X-rays used. However, model calculations with a complete ordering of Li and Ni yield much higher intensities for the superstructure reflections than actually observed. Thus, part of the domains must be *smaller* than the coherence lengths. By means of X-ray diffraction no distinction can be made between such a short-range order in microdomains and a pure statistical disorder on the metal positions. However, the presence of large domains and the spectroscopic results to be discussed in the following are convincingly in favor of the order model. In the structural refinement the short-range order in the microdomains is described by a partial location of Li and Ni on both metal sites 1 (2b) and 2 (2d) (average of scattering factors). For a complete long-range order the site occupation factors (SOF) Li:Ni would be 1:0 and 0:1 for sites 1 and 2, respectively, whereas for a totally "disordered" structure the value would be $\frac{1}{2}:\frac{1}{2}$ for both sites. On this basis an ordering parameter ω is defined (Eq. [1]), which reflects the percentage of long range ordered domains in the structure.

$$\omega = 2[\mathrm{SOF(Li1)} - \tfrac{1}{2}] \times 100\% \qquad [1]$$

The observed twinning of large domains is taken into account by calculating the F_c^2 values for a (110) twin (average of F^2 values), as defined in Eq. [2]. Here, indices hkl and $h'k'l'$ refer to A and B domains, respectively, while x is the twin ratio as calculated from the volumes V of domains A and B.

$$F_c^2(hkl)_{\mathrm{twin}} = (1 - x)F_c^2(hkl) + xF_c^2(h'k'l')$$
$$x = \frac{V(\mathrm{B})}{V(\mathrm{A}) + V(\mathrm{B})} \qquad [2]$$

The calculations were performed with the SHELXL program (14). The reflections compatible with A centering only were allotted to domain A, those compatible with B centering only to domain B, and the main structure reflections to both domains (18). Since the influence of the superstructure reflections, which is decisive for the determination of the twin ratio, and of the coordination geometries (via the cation ordering) as well, would be distinctly reduced by the usual weighting schemes, unit estimated standard deviations have been used for all reflections (modified SHELXL weighting scheme according to $w = 1/(1 + 0.1p^2)$, with $p = \max(F_o^2, 0 + 2F_c^2)/3$. Due to this procedure and to the necessity to refrain from averaging the intensities of equivalent reflections in the twin refinement, rather large residuals had to be accepted ($R_2 = 0.240$, $R = 0.071$, GOOF = 1.53). Seemingly better R values result after the averaging of the reflection intensities without utilizing the twin program and with program-optimized weights ($wR_2 = 0.082$, $R = 0.039$, GOOF = 1.25). In view of the strong pseudosymmetry, anisotropic displacement factors were refined only for the La atoms. To avoid correlations with the Li/Ni site occupation factors, equal isotropic displacement parameters were used for the Li and Ni atoms on the 2b and 2d positions. Test refinements of single occupation factors without stoichiometrical restrictions gave no significant deviations from the $La_2Li_{1/2}Ni_{1/2}O_4$ composition. The resulting atomic parameters for this mixed "twin" and "disorder" model are given in Table 3. The twin ratio (A in relation to B unit cell frequency) was found to be 0.80, the degree of long-range order ω is 74% (Table 3). On the basis of these results the probable structure of the second crystal showing diffuse streaks parallel c^* may be estimated as follows: the layers

TABLE 2
Measuring Conditions and Parameters for the X-Ray Analysis of the Compounds $La_2Li_{1/2}M_{1/2}$ (M = Co, Ni, and Cu)

	M = Co	M = Ni	M = Cu
		Crystal data	
Formula	$La_2Li_{1/2}Co_{1/2}O_4$	$La_2Li_{1/2}Ni_{1/2}O_4$	$La_2Li_{1/2}Cu_{1/2}O_4$
Crystal size (mm^3)	$0.06 \times 0.11 \times 0.03$	$0.21 \times 0.20 \times 0.02$	$0.1 \times 0.1 \times 0.25$
Absorption μ (mm^{-1})	25.34	25.56	25.73
Space group	*Ammm*, $Z = 4$	*Ammm*, $Z = 4$	*I*4/*mmm*, $Z = 2$ (pseudo cell)
Lattice parameters (pm)			
a	535.0(1)	530.99(2)	372.60(4)
b	535.2 (1)	5.30.99(2)	372.60(4)
c	1264.6(2)	1288.71(1)	1316.95(7)
Temperature (K)	293	293	293
D_c ($g \cdot cm^{-3}$)	6.87	6.86	6.85
		Data collection	
Diffractometer	P4(Siemens)	CAD4 (Enraf Nonius)	CAD4 (Enraf-Nonius)
Radiation		Mo$K\alpha$ graphite monochromator (71.073pm)	
Scan mode		ω-scan	
Scan angle (deg)	1	$0.76 + 0.63 \tan\Theta$	$0.44 + 0.61 \tan\Theta$
θ range (deg)	1.6–29.9; $+h, \pm k, \pm l$	1.6–30.4; $-h, \pm k, \pm l$	3.1–37.8; $\pm h, \pm k, +l$
Reflections, used/unique	1973/333	1442/343	555/183
		Computing	
Refinement (14, 15)	SHELXL96	SHELXL96	SHELXL93
Atomic scattering factors		For neutral atoms; $\Delta f'$ and $\Delta f''$ from (16)	
Absorption correction (17)	Numerical	Empirical with ψ scans	Empirical with ψ scans
Extinction correction (15)	$\varepsilon = 0.0036(3)$	$\varepsilon = 0.015(2)$	$\varepsilon = 0.051(6)$
Refinement method		Full matrix least squares, $\sum w(F_o^2 - F_c^2)$ minimized	
Number of parameters	20	20	14
$R_2(F^2)$, $R(F)$	0.098, 0.079	0.240, 0.071	0.095, 0.036
Goodness of fit	0.521	1.535	1.157
Max ratio shift/esd	0.00	0.07	0.00
$\Delta\rho_{max/min}$ ($e/Å^3$)	1.8, -3.6 at La	3.3, -5.7 at La	4.6, -3.9 at La

are largely ordered but in the *c* direction the stacking of A-type and B-type layers shows disorder. The maxima on the diffuse streaks at $c^*/2$ point to predominant order sequences of the P type corresponding to an alternating sequence of A and B unit cells along the *c* axis (Fig. 4). In the first crystal about three-fourths of the volume consists of large-size domains, with the remaining one-fourth consisting of small domains below the coherence limit. In the second crystal, part of the domains are of large size in the layer directions ((001) plane) but of small size perpendicular to the layer planes. Very probably the (001) planes separating A- and B-type domains are the twin boundaries, as illustrated in Fig. 4. A reduction of the thickness of the domains with $c' = 2c$ along the [001] direction would correspond to a continuous transition toward 1D disorder.

A neutron diffraction powder investigation was performed on the E3 diffractometer (BENSC) at the Hahn-Meitner Institute in Berlin in addition, and the data were refined utilizing the Rietveld method. The measurements confirmed the X-ray results but did not yield the expected higher precision in the positional parameters of oxygen. Thus we refrain from a discussion.

Crystal Structure of $La_2Li_{1/2}Co_{1/2}O_4$

For a crystal of the analogous Co(III) compound the film records and the intensity data of a measurement on a four-circle diffractometer revealed essentially the same features as in the case of the Ni compound. No diffuse streaks were observed and the superstructure reflections were remarkably weaker. The same data handling and structural model was used for the refinement of the structure, leading to final residuals $R_2 = 0.098$, $R = 0.079$, and GOOF = 0.52 (when averaging the intensities of equivalent reflections and without utilizing the twin program, $wR_2 = 0.067$, $R = 0.025$, and GOOF = 1.09). The atomic parameters are given in Table 3. The twin ratio is 0.75 and the degree of long-range order only $\omega = 35\%$.

TABLE 3

Atomic Positions, Isotropic Temperature Factors U_{iso} (10^{-17} m^2), and Site Occupation Factors (SOF in SHELX notation) for $La_2Li_{1/2}M(III)_{1/2}O_4$: M(III) = Ni (first line), Co (ω = 35%) (second line), and Co (ω = 48%) (third line)

Atom	Position	x	y	z	SOF	U_{iso}
La1	4i	0	0	0.13664(4)	0.25	7.5(5)
		0	0	0.13445(4)	0.25	8.0(2)
		0	0	0.13452(4)	0.25	7.6(2)
La2	4*j*	0.5	0	0.36398(4)	0.25	7.6(5)
		0.5	0	0.36475(4)	0.25	7.7(2)
		0.5	0	0.36481(4)	0.25	7.7(2)
Li(M)[a]	2*d*	0	0	0.5	0.0161(8)	5.1(5)
		0	0	0.5	0.0407(8)	9.8(3)
		0	0	0.5	0.0325(9)	9.7(3)
M(Li)[a]	2*b*	0.5	0	0	0.1089(8)	5.1(5)
		0.5	0	0	0.0843(8)	9.8(3)
		0.5	0	0	0.0925(9)	9.7(3)
O1	8*o*	0.2559(6)	0.2470(6)	0	0.5	5.5(3)
		0.2626(14)	0.2464(15)	0	0.5	9.1(6)
		0.2518(12)	0.2492(13)	0	0.5	9.0(6)
O2	4i	0	0	0.3218(7)	0.25	10.4(4)
		0	0	0.3171(5)	0.25	15.6(6)
		0	0	0.3195(5)	0.25	15.7(5)
O3	4*j*	0.5	0	0.1718(7)	0.25	7.2(3)
		0.5	0	0.1633(5)	0.25	3.8(3)
		0.5	0	0.1646(6)	0.25	7.4(4)

Ordering parameters ω, number N of observed superstructure reflections $>3\sigma$, and twin ratios

Compound	ω (%)	$N > 3\sigma$	Twin ratio
$La_2Li_{1/2}Ni_{1/2}O_4$	74.4(1.2)	509	0.80(7)
$La_2Li_{1/2}Co_{1/2}O_4$	35(1.5)	56	0.75(2)
$La_2Li_{1/2}Co_{1/2}O_4$	48(1.5)	56	0.69(2)

Anisotropic temperature factors (10^{-17} m^2) of La(III) for M(III) = Ni (first line), Co (ω = 35%) (second line), and Co (ω = 48%) (third line)

Atom	U_{11}	U_{22}	U_{33}
La1	7.1(7)	9.2(7)	6.3(6)
	7.1(3)	10.4(4)	6.5(3)
	7.2(4)	9.8(4)	5.9(3)
La2	8.5(7)	8.1(7)	6.2(6)
	9.6(4)	8.1(4)	5.5(3)
	8.8(4)	8.5(4)	5.7(3)

[a] Li(M) and M(Li) denote sites mainly occupied by Li(I) and M(III), respectively.

The refinement against the F^2 data converging at the minimum of $\sum w(F_o^2 - F_c^2)^2$ should—even with unit weights—still be mainly determined by the strong "basic structure" reflections. Thus, the minimization of $\sum(|F_o| - |F_c|)^2$ is expected to yield more realistic results for parameters depending on the superstructure, such as the occupation factors of the metal positions. Because no twin model program based on $|F|$ data was available to us, we used SHELXL (14) again but searched for the minimum of the conventional R value ($R = \sum||F_o| - |F_c||/\sum|F_o|$ for all reflections) from iterative refinements with fixed occupancy factors. Interestingly enough, the lowest obtained R value is distinctly smaller than that resulting when the R_2 value is minimal. The corresponding ordering parameter increased considerably to $\omega = 48\%$, the twin ratio being 0.69 (Table 3). The final atomic parameters for this run are also listed in Table 3. The reliability factors are $R_2 = 0.101$, $R = 0.077$, and GOOF = 0.53. As discussed in the next section, the higher ω parameter yields more realistic results, in particular for the Co–O and Li–O bond lengths.

If the same procedure is performed with the data of $La_2Li_{1/2}Ni_{1/2}O_4$, the lowest R value is found for ω = 72(1)%, which is identical with the value corresponding to the ΔF^2 minimum (ω = 74(1)%) within the error limit. This result is in accord with the much larger number of superstructure reflections in comparison to that for the Co compound (Table 3).

Partial replacement of La by Sr ($La_{2-x}Sr_xLi_{1/2}Co_{1/2}O_4$ mixed crystals) should be compensated for reasons of charge balance by a corresponding rise of the oxidation state of part of the Co atoms from Co(III) to Co(IV). A crystal of this type was investigated by a film camera and a four-circle diffractometer. The unit cell of the chosen crystal, determined from the strong main structure reflections, shows a very small decrease of both lattice constants by about 0.2% compared with those of the pure La compound. Apparently, the decreasing ionic radius on the 3*d* metal position (Co(III): 54.5pm; Co(IV): $\approx$45 pm) is largely compensated by the increase on the 9-coordinated site (La(II): 122 pm; Sr(II): 131 pm) (19). Because diffuse streaks along c^* were present, no further evaluations were undertaken.

$La_2Li_{1/2}Cu_{1/2}O_4$

Most single crystals showed just very weak superstructure reflections, as did powder samples in neutron diffraction experiments. Refinements were only successful in the space group type $I4/mmm$ (No. 139) of the regular K_2NiF_4 lattice, however, giving an average structure. The resulting positional parameters of La (0.3621(1)) and O (0.1819(7)) in the z direction have to be regarded as approximate, because the additional reflections were neglected. Nevertheless they give useful information (see next section).

III. DISCUSSION OF THE STRUCTURAL RESULTS

$La_2Li_{1/2}Ni_{1/2}O_4$

The metal-oxygen distances and the angles within the LaO_9, LiO_6, and NiO_6 polyhedra are listed in Table 4. The

TABLE 4
Spacings (pm) and Angles (deg) within the LaO_9, $Li(Ni)O_6$, and $Ni(Li)O_6$ Polyhedra for $La_2Li_{1/2}Ni_{1/2}O_4$[a]

La1			La2	
La1–O1	258.2(2)	4×	La2–O1	256.1(2)
La1–O2′ (short)	238.6(9)	1×	La2–O3′ (short)	247.6(9)
La1–O2	270.9(2)	2×	La2–O2	271.0(2)
La1–O3	269.3(2)	2×	La2–O3	269.5(2)
Li(Ni)			Ni(Li)	
Li(Ni)–O1	191.1(3)	4×	Ni(Li)–O1	184.4(3)
Li(Ni)–O2	229.6(10)	2×	Ni(Li)–O3	221.4(9)
La1 (Fig. 5, left)			La2 (Fig. 5, right)	
O1(1b)–La1–O1a(1c)	94.0(1)	2×	O1i(1h)–La2–O1j(1g)	93.6(1)
O1(1a)–La1–O1c(1b)	63.5(1)	2×	O1h(1i)–La2–O1j(1g)	63.3(1)
O1(1a)–La1–O1b(1c)	61.1(1)	2×	O1h(1g)–La2–O1i(1j)	60.8(1)
O2e–La1–O2f	157.2(4)	1×	O2–La2–O2l	156.8(4)
O3–La1–O3d	160.5(4)	1×	O3k–La2–O3h	160.2(4)
O2′–La1–O1(1a, 1b, 1c)	133.0(1)	4×	O3′–La2–O1h(1i, 1g, 1j)	133.2(1)
O2e–La1–O1a(1b)	129.3(2)	4×	O1h(1j)–La2–O2	129.3(2)
O2f–La1–O1(1c)			O1i(1g)–La2–O2l	
O2e–La1–O1(1c)	68.7(2)	4×	O1i(1g)–La2–O2	69.0(2)
O2f–La1–O1a(1b)			O1h(1j)–La2–O2l	
O2′–La1–O2e(2f)	78.6(2)	2×	O3′–La2–O2(2l)	78.4(2)
O1(1b)–La1–O3	129.3(2)	4×	O3h–La2–O1g(1j)	129.4(2)
O1a(1c)–La1–O3d			O3k–La2–O1h(1i)	
O1a(1c)–La1–O3	66.2(2)	4×	O3h–La2–O1h(1i)	66.5(2)
O1(1b)–La1–O3d			O3k–La2–O1g(1j)	
O2′–La–O3(3d)	80.3(2)	2×	O3′–La2–O3h(3k)	80.1(2)
O3–La1–O2e(2f)	88.1(1)	4×	O3h–La2–O2(2l)	88.0(1)
O3d–La1–O2e(2f)			O3k–La2–O2(2l)	
Ni(Li)			Li(Ni)	
trans			trans	
O1–Ni(Li)–O1	180	3×	O1–Li(Ni)–O1	180
O2–Ni(Li)–O2			O3–Li(Ni)–O3	
cis			cis	
O1–Ni(Li)–O1	89.4(2)	2×	O1–Li(Ni)–O1	89.3(2)
	90.6(2)	2×		90.7(2)
O1–Ni(Li)–O2	90	8×	O1–Li(Ni)–O3	90

[a] For the notations of the O–La–O angles, see Fig. 5.

averaged La1–O and La2–O spacings are 261.3(3) and 261.5(3) pm, respectively, and correspond exactly to those calculated from tabulated ionic radii (261.6 pm), if the—here valid—value for six-coordinated O^{2-} (1.40 Å) is used (19). Figure 5 illustrates the oxygen coordinations of the two crystallographically different La(III) ions, giving the key for the listed La–O spacings and O–La–O angles (Table 4). The LaO_9 polyhedra are essentially strongly distorted Archimedes antiprisms with one capped face (by O2′ and O3′ for La1 and La2, respectively). The metal ions are displaced considerably from the polyhedron centers toward the more extended $(O2)_2(O3)_2$ planes, inducing slightly smaller spacings to the O1 atoms, which constitute the less extended plane of the antiprism.

From the (Ni,Li)–O spacings on the two different octahedral positions and the respective occupation numbers (Table 3, Eq. [1]), we can extrapolate the Ni–O and Li–O spacings in the completely ordered compound to be 183 (4×), 220 pm (2×) and 192 (4×), 231 pm (2×), respectively (Table 6). The average Ni–O bond length is $195._5$ pm, which should be compared with the expected ionic radii sums for low-spin (196 pm) and high-spin Ni(III) (200 pm) and for low-spin Ni(IV) (188 pm) as well (19). Without doubt, nickel is present in $La_2Li_{1/2}Ni_{1/2}O_4$ in the low-spin +III oxidation state, possibly with a tiny admixture of low-spin Ni(IV). This result is confirmed by EPR spectroscopy, the magnetic investigation (see Section IV), and the analytical data. Both the NiO_6 and the LiO_6 octahedra exhibit a considerable tetragonal elongation. The radial distortion parameter (20), defined in Eq. [3], is $\rho \cong 43$ pm for the NiO_6 polyhedron and $\rho \cong 45$ pm for the LiO_6 polyhedron.

$$\rho = \{2(\delta a_x^2 + \delta a_y^2 + \delta a_z^2)\}^{1/2}$$

[δa_i: deviations of the M–O bonds from the average octahedral spacing] [3]

One reason for the pronounced local distortions is the contrapolarizing action of the La(III) cations.The O(2) and O(3) ligand atoms, which are axially bonded to Li and M (Ni, Co, Cu), respectively, possess cationic coordinations O(2)[LiLa(1)$(La(2))_4$] and O(3)[MLa(2)$(La(1))_4$] with pseudooctahedral C_{4v} symmetry and linear LiO(2)La(1) and MO(3)La(2) entities (see Fig. 3). The O(2) and O(3) centers lie distinctly above the La_4 planes, shifted torward the axial La atom. It is thus the contrapolarizing effects of the (1 + 4) La(III) cationic sphere on the M(III)–O(3) and Li(I)–O(2) bonds which lead to an axial elongation of the MO_6 polyhedron and in particular the LiO_6 polyhedron. Similar considerations are valid for the O(1) atoms, which are involved in the equatorial bonds toward M(III) and Li(I). They possess an O(1)[MLiLa$_4$] cationic coordination again with C_{4v} symmetry. However, here the oxygen atoms only slightly deviate (< 10 pm) from the La_4 plane perpendicular to the linear MO(1)Li entity. Thus we expect a strong polarizing effect of M(III) on the Li–O bond with a contraction of the M–O(1) spacings. In the case of M = Ni(III) a distortion component caused by vibronic Jahn–Teller coupling in the ^2E_g ($t_{2g}^6 e_g^1$) ground state (Section IV) is expected to add to the tetragonal elongation due to the host site strain. Indeed the radial distortion parameter of Ni(III) is considerably larger than that of Co(III) ($\rho \approx 18(5)$ pm), as outlined later.

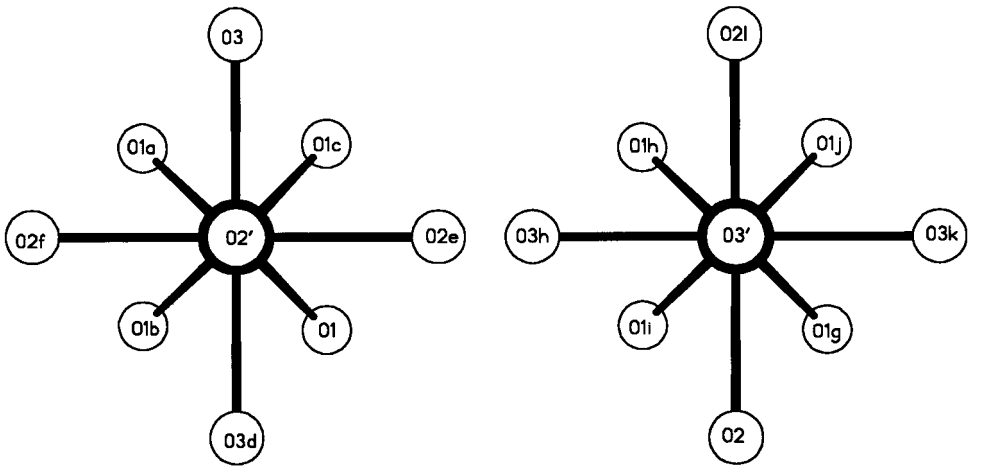

FIG. 5. LaO_9 coordination polyhedra of La1 (left) and La2 (right), with the bond lengths and angles listed in Table 4.

We would like to mention here that the superstructure of the K_2NiF_4-type compounds $La_2Li_{1/2}M_{1/2}O_4$ closely resembles that of K_2CuF_4. In the latter compound the CuF_6 polyhedra, which are strongly distorted due to vibronic coupling, exhibit an antiferrodistortive cooperative-elastic Jahn–Teller order (20, 21). This order pattern implies a considerable shift of the fluoride anions, which bridge two Cu^{2+} ions in the (001) planes, from their special positions in the K_2NiF_4 structure, leading to structural effects (22) similar to those just discussed. In the oxidic solids considered here, it is not the anion shift alone, but the presence of two different cations as well, which induces the superstructure, however.

$La_2Li_{1/2}Co_{1/2}O_4$

Table 5 displays the metal–oxygen spacings within the LaO_9, Co(Li)O_6, and Li(Co)O_6 polyhedra for the ordering parameters $\omega = 48\%$ and 35%. Though the metal–oxygen spacings do not differ much in the two cases, the Ni–O and Li–O spacings extrapolated to those characteristic for a complete cation order are very different. For $\omega = 48\%$ more reasonable bond length data are obtained (compare Section II). The averaged La1–O (260.1 pm) and La2–O (262.2 pm) distances again compare well with the value from the ionic radii (261.6 pm). The Co–O and Li–O spacings, extrapolated from the bond lengths listed in Table 5, are 187 (4×), 198 pm (2×) and 191 (4×), 238 pm (2×), respectively. The average Co–O spacing is $190._5$ pm, as compared to values of $194._5$ pm for low-spin Co(III) and 201 pm for high-spin Co(III) deduced from reported ionic radii (19). The average Co–O bond length extrapolated for $\omega = 35\%$, on the other hand, is 183 pm—representing an unrealistically short spacing. As expected, the geometry of the LiO_6 octahedron is similar in the nickel and cobalt solids. Adopting the Li–O bond length from $La_2Li_{1/2}Ni_{1/2}O_4$, where the extrapolated spacings are more reliable, we obtain Co–O distances of 186 (4×) and 205 pm (2×), with an average of $192._5$ pm (Table 6). Evidently, also in this case the trivalent transition metal ion appears in the low-spin state, but obviously with a small fraction of low-spin Co(IV)—possessing $a \approx 10$ pm smaller ionic radius—admixed (see Section IV). The distortions of the LiO_6 and CoO_6 polyhedra (≈ 45 and $\approx 18(5)$ pm, respectively) are induced exclusively by lattice strains, as discussed earlier. Co(III) possesses an orbitally nondegenerate $^1A_{1g}$ (t_{2g}^6) ground state in octahedral coordination, which is Jahn–Teller stable in contrast to Ni(III).

TABLE 5
Metal-to-Ligand Spacings (pm) in $La_2Li_{1/2}Co_{1/2}O_4$ for $\omega = 35\%$ and $\omega = 48\%$

	$\omega = 35\%$	$\omega = 48\%$	
La1–O1	254.1(6)	254.7(5)	4×
La1–O2′ (short)	230.9(6)	234.0(7)	1×
La1–O2	274.5(2)	273.8(2)	2×
La1–O3	270.0(2)	270.2(1)	2×
La2–O1	255.3(6)	254.7(5)	4×
La2–O2	274.2(2)	273.6(1)	2×
La2–O3′ (short)	254.8(6)	253.2(7)	1×
La2–O3	269.9(1)	270.2(1)	2×
Co(Li)–O1	191.5(8)	190.2(7)	4×
Co(Li)–O2	231.4(6)	228.2(7)	2×
Li(Co)–O1	186.8(8)	188.2(7)	4×
Li(Co)–O3	206.4(6)	208.2(7)	2×

$La_2Li_{1/2}Cu_{1/2}O_4$

The average (Li,Cu)–O spacings estimated from the positional parameters (see Section II) are 186(1) (4×) and

239(1) pm (2×). Assuming Li–O bond lengths as derived for the Ni compound, the Cu–O distances in Table 6 result. They indicate an extremely pronounced tetragonal elongation ($\rho \approx 78$ pm), implying a square-planar coordination with only rather weak bonds in the axial directions. Such a D_{4h} (nearly square-planar) geometry is expected to be correlated with a low-spin configuration of Cu(III) and spin pairing in the octahedral e_g orbitals $(d_{z^2})^2$ and $(d_{x^2-y^2})^0$. Indeed the equatorial Cu–O distances of 180 pm are comparable to those reported for the planar CuO_4 units in $KCuO_2$ [184 pm (23)] and $KNa_4[Cu(HIO_6)_2]\cdot 12H_2O$ [183 pm (24)]. The coordination sphere in the latter compound is supplemented by two axial H_2O molecules at a distance of >2.7 Å. We have refined the latter structure and could confirm the published results, though with distinctly improved reliability factors [Cu–O spacings: 184.2(3), 183.4(3) (2×), and 183.6(3) pm, with angles between the Cu–O bonds deviating by $< 7^\circ$ from 90°]. The two mentioned structures of oxidic copper(III) compounds are the only ones reported in the literature based on single-crystal X-ray analyses. The low-spin configuration of Cu(III) in $La_2Li_{1/2}Cu_{1/2}O_4$ is also suggested by the magnetic investigation and EPR spectroscopy. The electronic structure of copper in comparison to nickel and cobalt in compounds $La_2Li_{1/2}M_{1/2}O_4$ (M = Cu, Ni, Co) is discussed in the next section.

A single-crystal X-ray structure analysis of $Nd_2Li_{1/2}Cu_{1/2}O_4$, which we performed, yielded similar results, with slightly reduced (Li,Cu)–O spacings due to the substitution of La(III) by the smaller Nd(III) cation. As for the La compound only very weak superstructure reflections were observed.

We did not find any indication for the existence of the Nd_2CuO_4 structural type (25), in which the O(2) atoms occupy the 4*d* positions in *I*4/*mmm*. This structure might have been suggested, because the *M*(III) cation is found here in a square-planar coordination—a geometry which is mostly observed for low-spin d^8 cations. Indeed $La_2Li_{1/2}Au_{1/2}O_4$ (9) with low-spin $5d^8$ configured Au(III) adopts this lattice type in its ordered version.

TABLE 6

Extrapolated *M*–O and Li–O Bond Lengths (pm) in Solids $La_2Li_{1/2}M_{1/2}O_4$ from Data in Tables 4 (Ni), 5 (Co, ω=48%)[a], and for *M*=Cu

M	*M*–O		Li–O		
Ni	183 (4×),	220 (2×) (43)	192 (4×),	231 (2×)	(45)
Co	187 (4×),	198 (2×) (13)[b]	191 (4×),	238 (2×)	(54)
Cu	≅180 (4×),	≅247 (2×) (78)[c]			

[a]The radial distortion parameters ρ (pm) of the MO_6 and LiO_6 polyhedra are given in parentheses.

[b]Adopting the Li–O spacings for *M* = Ni: 186(4×), 205 (2×) (22).

[c]Adopting the Li–O spacings for *M* = Ni.

IV. SPECTROSCOPIC AND MAGNETIC RESULTS

A. Electronic Structure of the Transition Metal Ions

Cobalt. The EPR spectrum of the cobalt compound shows the typical features of a cation with the low-spin t_{2g}^5 configuration in a tetragonally elongated octahedral coordination. Apparently, the transition metal ion, which is predominantly in the EPR-silent low-spin Co(III) state, contains a significant fraction of low-spin Co(IV). This is in agreement with the experimental oxidation state determination, indicating a distinctly higher average value than + III and a smaller ionic radius than that of low-spin Co^{3+} (see Sections II and III). The spectrum is clearly orthorhombic, which may be readily explained by an inhomogeneous distribution of Li(I) ions in the neighborhood of a paramagnetic Co(IV) center because vacancies on the Li positions have to be assumed for reasons of charge compensation [$La_2Co_{1/2}Li_{1/2-\delta}O_4$; $\delta \triangleq$ Co(IV)]. Increasing the Co(IV) concentration in $La_{2-x}Sr_xLi_{1/2}Co_{1/2}O_4$ mixed crystals washes out the hyperfine structure and broadens the signals, without destroying the main spectral features. A thorough discussion of the observed spectral features will be given elsewhere (26). A spectrum of the compound with $x = 0.5$ has already been reported (7).

The question whether Co(III) occurs in the high- or low-spin configuration in ceramic oxides is still controversially discussed and will be considered from a rather general standpoint in the following. In Table 7 ligand field parameters are collected, deduced from the *d*–*d* spectra of the $3d^n$ cations Cr(III), Co(III), Ni(III), and Cu(III) in an octahedral field of fluoride and oxide ions. In the case of oxygen only data for Cr(III) are available (27), whereas for the cations Co(III) to Cu(III) the metal–oxygen bond is already covalent to such an extent that the *d*–*d* transitions are partly or even completely obscured by low-lying charge transfer bands. Hence ligand field parameters cannot be deduced

TABLE 7

Ligand Field Parameters Δ (10^3 cm^{-1}) and Nephelauxetic Ratios β ($= B/B_0$) for 3*d* Cations *M*(III) in an Octahedral Coordination of Fluoride (Left Three Columns) and Oxide Anions[a] (Columns 4–6) and Racah Parameters for the Free Ions (B_0, in 10^3 cm^{-1}) (28)

M(III)	Δ	β	Δ/*B*	Δ^b	β^b	Δ/B^b	Ref	B_0
Cr	16.1	0.84	20.7	16.8 (±0.7)	0.65 (±0.08)	$28_{.5} \pm 2$	27	0.92
Co	13.1	0.72	16.6	13.7 (±0.6)	0.56 (±0.07)	23 ± 2	28	1.09
Ni	13.9	0.65	18.5	14.5 (±0.6)	0.50 (±0.06)	26 ± 2	29	1.15
Cu	14.1	0.53	21.7	14.7 (±0.6)	0.41 (±0.05)	29 ± 2	28	1.21

[a] Isomorphic substitution of an *M*(III) ion of comparable size (such as Ga(III)) in various oxide ceramics.

[b]Values for Co(III), Ni(III), and Cu(III) are estimated by extrapolation from the Cr(III) values (see text).

from experiment but have been extrapolated (Table 7) from the fluoride data on the basis of the trend observed for Cr(III) when switching from the F^- ligand to the oxygen ligator atoms (27). This procedure follows a concept of Jørgensen, who defines Δ as the product of increments due to the anion (f) and the cation (g) [$\Delta \equiv f \cdot g \cdot 10^3\ cm^{-1}$] and similarly the relative decrease of B with respect to the free-ion value [$\beta = B/B_0$] by a product of h and k, standing for the anionic and cationic contribution, respectively [$1 - \beta \equiv h \cdot k$] (30). For example, we obtain from $h(F^-) = 0.8$ and the values $k(Cr^{3+}) = 0.20$ and $k(Co^{3+}) = 0.33$ β ratios of 0.84 and 0.73_5, respectively, in good agreement with the corresponding experimental values in Table 7. The cited nephelauxetic ratios β refer roughly to the nephelauxetic parameter B_{35} in the Jørgensen nomenclature (30), which is connected with the change in the interelectronic repulsion when exciting an electron from the antibonding t_{2g}^* into the σ-antibonding e_g^* MO. They indicate a drastic covalency increase and stability decrease, proceeding from Cr(III) to Co(III) to Ni(III) and finally to Cu(III).

Oxygen is a very exotic ligator atom, whose bonding properties toward a probe cation vary widely depending on its specific further cationic coordination. Hence the Δ and β values strongly depend on the chemical constitution (the number, charge, and electronic configuration of the contrapolarizing cations) and the structure of the oxide ceramic (27, 31), inducing a range of Δ and β parameters (Table 7) which can no longer be taken into account by a single f and h increment in the Jørgensen factorization.

It is seen from the data in Table 7 that the Δ/B ratio of Co(III) is distinctly below the critical value of 20.0 (with $C/B = 4.8$) for F^-, which marks the high-spin–low-spin crossover in the d^6 Tanabe–Sugano energy diagram. Switching to H_2O as the ligand yields $\Delta/B = 19.3$, very near the critical ratio, but still in the high-spin region. In oxide matrices we expect Δ/B ratios larger than about 21, regarding the extrapolated parameters for the Co(III)–O bond in Table 7 (right) as reliable estimates. One may conclude on the basis of the optical data that Co(III) in ceramic oxides and octahedral coordination should in general be low-spin configured with a $^1A_{1g}(t_{2g}^6)$ ground state. This conclusion is in accord with the structural data in Section II.

It is suggested on the basis of magnetic susceptibility data (4, 8) that a thermally accessible intermediate spin state ($S = 1$) of Co(III)—stabilized by the tetragonal ligand field—is populated at higher temperatures. Our own magnetization measurements at 50 G between 3 and 25 K indeed indicate the presence of a small fraction of local spins, which order antiferromagnetically. However, we prefer an interpretation assuming a low-spin Co(IV) admixture, which is supported by EPR spectroscopy and by the analytical data.

For the parameter set $B \cong 610\ cm^{-1}$, $\Delta/B \cong 23$ (Table 7) the first two spin-allowed transitions $^1A_1 \rightarrow {}^1T_1, {}^1T_2$ of Co(III) are estimated to occur at about 13,300 and 20,300 cm^{-1}, respectively, from the respective Tanabe–Sugano diagram. The powder reflection spectrum shows a gentle intensity increase from the near-IR to the charge-transfer region starting around 19,000 cm^{-1}, superimposed by a distinct maximum at $\cong 13{,}500\ cm^{-1}$, in essential agreement with the expectation.

Nickel. The Ni(III) centers in $La_2Li_{1/2}Ni_{1/2}O_4$ are low-spin configured, as is unambiguously deduced from the EPR spectrum (5, 32) and also in accord with the structural results. The presence of a tiny percentage of Ni(IV) cannot be excluded, because this cation is EPR silent in the low-spin state [$^1A_{1g}(t_{2g}^6)$]. Though the Δ/B ratio for NiF_6^{3-} polyhedra (18.5) is considerably smaller than the critical value of 22.6 for the spin crossover in the d^7 Tanabe–Sugano diagram (with $C/B = 4.9$) (Table 7, left), Ni(III) is already low-spin configured in fluoride host lattices. It has been demonstrated (29, 32) that it is the energy gain by vibronic Jahn–Teller coupling (tetragonal elongation of the NiF_6^{3-} octahedron), which stabilizes a low-spin ground state [$^2A_{1g}(d_{z^2})^1$]. For Ni(III) in oxidic compounds the Δ/B ratios seem to be larger (> 24) than the critical value (Table 7); thus here the high-spin to low-spin conversion does not necessarily need energetic assistance by the Jahn–Teller effect. We conclude that Ni(III) in oxide ceramics is always low-spin configured, provided that the paramagnetic centers are isolated from each other in the host lattice, as in the case under discussion. In the presence of cooperative electronic interactions, however, the electronic states broaden into bands, and with the critical condition that the bandwidth is larger than the energy difference between the low-spin ground state and the first excited quartet term, a spin flip to the high-spin configuration eventually occurs (32).

Using the Δ parameter of $\cong 14{,}600\ cm^{-1}$ suggested for the Ni(III)–O bond (Table 7) and the experimental Ni–O bond lengths (Table 6), one can estimate the ^2E_g ground state splitting $4E_{JT}$ on the basis of angular overlap (AO) considerations and assuming that Δ varies reciprocally with the fifth power of the metal–ligand spacing. One obtains $4E_{JT} \cong 10{,}800\ cm^{-1}$ [$^2A_{1g} \rightarrow {}^2B_{1g}$], and the next spin-allowed transition is expected not below 16,500 cm^{-1}.

The powder reflection spectrum is similar to that of the Co(III) solid, but with a distinct shoulder at $\cong 10{,}000\ cm^{-1}$ and a further less resolved shoulder around 17,500 cm^{-1}, both features imposed on the low-energy slope to the charge-transfer absorption. These energies are also in accord with the AO estimations.

The $1/\chi$ and μ_{eff} versus temperature plots (Fig. 6) are similar to those published before (5) and indicative of a paramagnetic solid with a μ_{eff} value of 1.50 μ_B, which is nearly 20% smaller than the expected magnetic moment ($S = \frac{1}{2}$, $g \cong 2.14$, $\mu_{eff} \cong 1.85\ \mu_B$). Below 40 K very weak spin–spin correlations of the antiferromagnetic type seem to

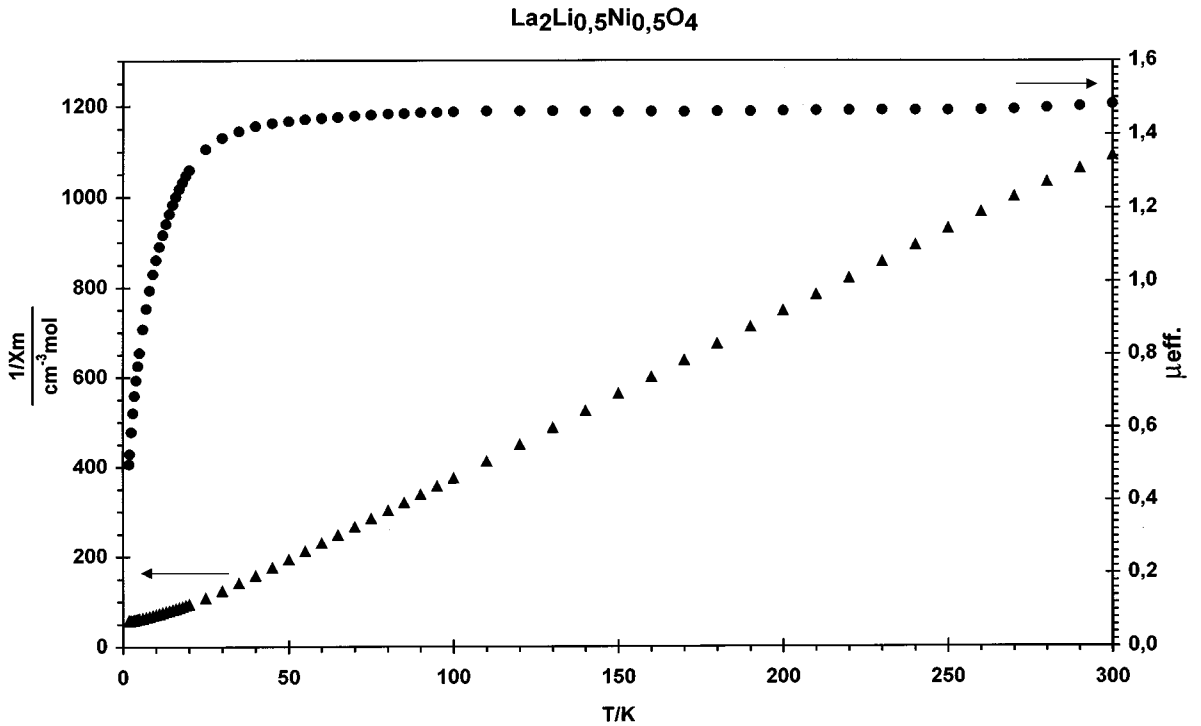

FIG. 6. Plots of the reciprocal magnetic susceptibility and of the effective magnetic moment (in units of μ_B) versus temperature for $La_2Li_{1/2}Ni_{1/2}O_4$.

be present, with $\theta_p \cong -2(2)$ K being negligibly small. Apparently, the order is not long range, because EPR signals are observable down to 4 K. The reduction of the magnetic moment could be due to the presence of a small fraction of diamagnetic low-spin Ni(IV) (see the preceding discussion under "Cobalt") and/or a tiny disorder on the octahedral sites with spin-coupled Ni(III)–O–Ni(III) superexchange pairs ($S = 0$). Thus the magnetic results support the concept of a complete (or nearly complete) cation order between Ni(III) and Li(I) and confirm the low-spin configuration of Ni(III) as well.

Copper. Copper(III) in an octahedral fluoride coordination is high-spin configured [$^3A_{2g}$ ($t_{2g}^6 e_g^2$) ground state; $\Delta = 14{,}100\ \text{cm}^{-1}$, $B = 640\ \text{cm}^{-1}$] (28), placing the first excited singlet term $^1_aE_g(t_{2g}^6 e_g^2)$ at $E_{31} \cong 8B + 2C \cong 11{,}100\ \text{cm}^{-1}$ (with $C/B = 4.7$) above the ground state in the strong-field approximation. It is this term which strongly splits by a tetragonal elongation, thus eventually stabilizing a singlet ground state $^1_aA_{1g}$, originating from the $^1_aE_g$ parent term. On the basis of the β trend, switching from fluoride to oxide as the ligand (Table 7), E_{31} can be estimated to decrease by about 2500 cm^{-1}. Hence a splitting of the excited ^1E_g state by $\approx 18{,}000\ \text{cm}^{-1}$—induced by vibronic Jahn–Teller coupling and the host site strain—would already suffice to transform Cu(III) into the low-spin configuration. This critical condition is apparently met, as indicated by the extremely strong D_{4h} ligand field with only weakly bonded axial oxygen atoms. The optical spectrum is empty up to 17,000 cm^{-1}, the onset of the charge-transfer absorption.

Though a square-planar coordination does not necessarily indicate a low-spin configuration for the d^8 cation [the NiO_4 entity in Li_2NiO_2 possesses an $S = 1$ ground state (33)], Cu(III) is low spin in $La_2Li_{1/2}Cu_{1/2}O_4$ because the compound is diamagnetic (3) (our own magnetic measurements confirm this result) and accordingly the EPR spectrum does not show a signal down to low temperatures.

B. Valence State Considerations

There is an ongoing controversy between chemists and physicists about the nature of oxo-coordinated copper in the oxidation state + III, which, in our opinion, is caused by the different bonding models used rather than by largely diverging interpretations. The one-electron ground state of Cu(II) in the usual Jahn–Teller-induced tetragonally elongated octahedral coordination is (beyond the closed d^8 configuration) $b_{1g}^2 b_{1g}^{*1}$, where both MOs—the bonding b_{1g} and the antibonding b_{1g}^*—transform as $d_{x^2-y^2}$ in D_{4h}.

The respective MO wavefunctions are given in Eq. [4].

$$\psi(b_{1g}^*) \cong \alpha d_{x^2-y^2} - \alpha' L_{x^2-y^2}$$

$$\psi(b_{1g}) \cong \alpha' d_{x^2-y^2} + \alpha L_{x^2-y^2} \qquad [4]$$

Here, $L_{x^2-y^2}$ is the symmetry-adapted linear combination of ligand orbitals (LCAOs), and α and α' are mixing coefficients ($\alpha^2 + \alpha'^2 \cong 1$). α has been determined by EPR spectroscopy to be $\cong 0.92$ and $\cong 0.87(2)$ for F^- ligands and O ligator atoms, respectively (34), indicating bonds which are about 85 and 75% ionic. In the nomenclature of physicists involved in X-ray photoemission and absorption spectroscopy—using a hole formalism for the ligand contributions ($\underline{L}$)—$d_{x^2-y^2}$ and $L_{x^2-y^2}$ in Eq. [4] would correspond to d^9 and $d^{10}\underline{L}$.

In the case of Cu(III) in square-planar oxo-coordination it is suggested (35) that the ground state is $d^9\underline{L}$ with a small, but significant $3d^8$ contribution. This is interpreted as Cu^{2+} with nearly one electron hole at oxygen, which gives rise to misunderstandings from the side of chemists. However, looking more closely at the ground state of low-spin Cu(III) in the MO hole description, namely $\underline{b_{1g}^{*2}}$, the apparent contradiction is resolved. Choosing $\alpha \geq 1/\sqrt{2}$ and $\alpha' \leq 1/\sqrt{2}$(Eq. [4]), one obtains $d^9\underline{L}$ ($+d^8$), indicating a pronounced d covalency of the Cu(III)–O bond with (approximately) maximum hole delocalization in the σ-antibonding b_{1g}^* MO, quite in accord with chemical experience. As a consequence of the double degeneracy of the b_{1g}^* state, each of the two electron holes in this MO apparently possesses about 50% probability density at the ligand. This indeed corresponds to the nearly total transfer of one electron from the ligand to the $3d$ metal by covalence. An interpretation of the valence state as being approximately "Cu^{2+}–O^-" is strongly misleading, however.

We should also mention that the given simple bonding concept is only valid if the considered CuO_4 or CuO_6 clusters are isolated from each other as in the compound $La_2Li_{1/2}Cu_{1/2}O_4$. Otherwise extended charge transfer may take place (36), involving more than one Cu center and thus creating itinerant holes, which may have different properties from those of isolated polyhedra, broadening the local Cu(III) states into bands.

Similarly, Ni(III) ceramic oxides are much more covalent than oxidic Ni(II) solids, though the extent of covalency in the former compounds is less pronounced than in the case of Cu(III) (37). This is in agreement with the redox instabilities, which increase in the sequence Co(III), Ni(III), Cu(III). The latter result further reflects that the d-covalency of the M(III)–O bond is less pronounced for Co(III) than for Ni(III). Here even Co(IV) can be stabilized in $La_{3/2}Sr_{1/2}Li_{1/2}Co_{1/2}O_4$ (7, 8).

C. IR Evidence

The increase of the tetragonal elongation of the MO_6 octahedra in the sequence Co(III), Ni(III), Cu(III) is nicely mirrored by the IR spectra. In the region where the M–O vibrations are expected, two rather narrow bands $\bar{\nu}_1$ and $\bar{\nu}_2$—the former being more intense—appear (Fig. 1), which can be readily assigned to the $E_u(1)$ and $A_{2u}(1)$ split modes of the octahedral $T_{1u}(1)$ stretching vibration for a tetragonally elongated geometry, respectively (Table 8). With increasing distortion, $E_u(1)$ shifts to higher energies and $A_{2u}(1)$ to lower energies, as expected, and accordingly the energy difference $\bar{\nu}_1 - \bar{\nu}_2$ becomes larger in switching from Co (130 cm^{-1}) to Ni (156 cm^{-1}) and finally to Cu (182 cm^{-1}). The assignment is supported by looking at the weighted averages of the split-band energies, which are 631, 640, and 646 cm^{-1} for the three cations, with slightly decreasing ionic radii in the sequence Co(III), Ni(III), Cu(III). A third band is observed around 450 cm^{-1} ($\bar{\nu}_3$). It is rather broad in the case of Co(III) and might be assigned to the $T_{1u}(2)$ bending vibration with an unresolved splitting into the $A_{2u}(2)$ and $E_u(2)$ component at higher and lower energy, respectively. Though speculative, the assignment is supported by the spectrum of $La_2Li_{1/2}Cu_{1/2}O_4$ (Fig. 1), where the $\bar{\nu}_3$ absorption has lost intensity and is very sharp, while $\bar{\nu}_2$ is much more intense now. The intensity gain of the latter band might be due to the overlap with the $A_{2u}(2)$ mode, $\bar{\nu}_3$ being the well-separated $E_u(2)$ component now (splitting: ≈ 85 cm^{-1}).

V. DISCUSSION AND CONCLUSIONS

Though twinning and/or disorder effects in the stacking sequence along the crystallographic c direction make the structural refinement rather difficult, the spectroscopic evidence supports the interpretation of a complete (or nearly complete) cation order between Li(I) and M(III) in the (001) layers of the compounds $La_2Li_{1/2}M_{1/2}O_4$ (M(III) = Co, Ni, Cu). Although the superstructure of the K_2NiF_4-type unit cell in the (001) plane according to $a = b = a_0\sqrt{2}$ is well established, diffuse streaks along c^* with maxima indicating $c = 2c_0$ can sometimes also be observed, somewhat

TABLE 8

***M*–O Vibrations[a] $\bar{\nu}_1$, $\bar{\nu}_2$, and $\bar{\nu}_3$ (cm^{-1}) in the IR Spectra of Compounds $La_2Li_{1/2}M_{1/2}O_4$ and Radial Distortion Parameters ρ (pm) of the MO_6 Polyhedra**

M	$\bar{\nu}_1$	$\bar{\nu}_2$	$\bar{\nu}_3$	ρ
Co	674	544	465	$\approx$ 18(5)
Ni	692	536	454	43
Cu	707	525	441	$\approx$ 78

[a] See text for assignments.

depending on the preparation conditions for the single crystals. Though the space group of the enlarged cell is orthorhombic, the metric remains tetragonal. The lattice is very similar to that of K_2CuF_4, where anion displacements due to antiferrodistortively ordered elongated CuF_6 octahedra (21) induce the superstructure (22). The cation order on the octahedral positions is further supported by the extrapolated geometries of the $M(III)O_6$ polyhedra. The tetragonal elongation increases strongly along the sequence Co to Cu, as expected when switching from a vibronically stable electronic configuration (Co) to a Jahn–Teller unstable ground state (Ni) and finally to a low-spin d^8 configuration (with strongly delocalized electrons in the σ-bonding b_{1g} ($d_{x^2-y^2}$) orbitals), displaying a distinct tendency to adopt a square-planar coordination (Cu).

The MO_6 geometries for the three $3d^n$ cations ($n = 6$–8) are listed in Table 9, together with those for other M(III) cations. X-ray powder data are available for the solids $La_2Li_{1/2}M_{1/2}O_4$ with M(III) = Al (10), Ga (11), and Mn (12), which are structurally described in terms of a disordered K_2NiF_4 lattice. Assuming that a superstructure analogous to that of the compounds with Co, Ni, and Cu is present, the MO_6 polyhedron distortion can be estimated if the equatorial Li–O spacings are 191 pm as derived from the structural results for Ni and if the Shannon ionic radii (19) are regarded as reliable (Table 9). It is nicely seen that the Mn(III) cation induces a very pronounced polyhedron elongation. It is obviously high-spin configured, possessing a strongly Jahn–Teller unstable ^5E_g ($t_{2g}^3e_g^1$) ground state in O_h symmetry. The radial distortion parameter ρ is much larger than for Al, Ga, and Co, where only the host site strain (vide supra) is present. If the equatorial Li–O distance is chosen somewhat shorter in the compounds which contain M(III) cations with larger ionic radii (Ga, Mn)—due to a weaker contrapolarizing effect of these cations on the Li–O bonds in the (001) planes—the polyhedron distortions measured by ρ (Eq. [3]) seem to be more realistic and follow rather closely the sequence of the c_0/a_0 ratios.

For the MnF_6^{3-} polyhedron, ligand field data of $\Delta = 14{,}300\ cm^{-1}$, $\beta = 0.80$, and $\Delta/B = 18.3$ are reported (38). Using arguments analogous to those in connection with the Δ and B parameters listed in Table 7, we deduce Δ/B ratios of 25 ± 2 for octahedrally coordinated Mn(III) in oxide ceramics, close to the Δ/B ratio of 27 ($C/B = 4.6$), which characterizes the high-spin to low-spin transition for a d^4 cation. Because the vibronic Jahn–Teller strongly stabilizes the high-spin configuration by a D_{4h} distortion, however, a $S = 2$ ground state is indeed expected.

$La_2Li_{1/2}Au_{1/2}O_4$, first described by Abbatista *et al.* (39), crystallizes in an ordered Nd_2CuO_4 structure with planar LiO_4 and AuO_4 entities (9) (Table 9), in contrast to ref. 39, where a superstructure of the K_2NiF_4 type (from X-ray powder diffraction data) is claimed for the gold compound. The reason Au(III) favors a Nd_2CuO_4-type structure where-

TABLE 9
M(III)–O Bond Length Data (pm)[a] and c_0/a_0 Ratios (Superstructure Not Taken into Account) for Compounds $La_2Li_{1/2}M_{1/2}O_4$

M(III)	eq (4×)	ax (2×)	ρ^b	r^c	c_0/a_0	Ref
Co	187	209	26	$54._5$	3.33_5	—
Ga[d]	190(194)	226(218)	42(28)	62	3.35_5	11
Al	186	208	25	$53._5$	3.38	10
Mn	188(192)	237(229)	57(43)	$64._5$	3.42	12
Ni	183	222	45	56	3.43	—
Cu	180	≈ 247	≈ 78	–	3.54	–
Au[e]	201	–	–	68	–	9

[a] M–O spacings estimated from the reported a_0 unit cell parameters and reported ionic radii (with $r(O^{2-}) = 140$ pm) with the assumption of equatorial Li–O spacings of 191 and, in parentheses, 187 pm
[b] ρ (pm): radial distortion parameter.
[c] r (pm): Octahedral ionic radii (square planar for Au) (19).
[d] Not entirely pure high-pressure phase: $a_0 = 381$ pm, $c_0 = 1278$ pm (11).
[e] Ordered Nd_2CuO_4 structure with square-planar AuO_4 and LiO_4 entities; Li–O spacings of 206 pm.

as Cu(III) prefers the K_2NiF_4 lattice—though both cations possess a low-spin d^8 configuration with a pronounced tendency toward a square-planar coordination—is possibly partly of geometrical nature. Recently, it has been suggested (40) that the K_2NiF structure type is favored for values of the tolerance factor t (Eq. [5]) larger than 1.0 and the Nd_2CuF_4 lattice (25) is favored for $t < 1$.

$$A_2BO_4\text{: } t = [3\sqrt{2}\ r_O + 2\sqrt{6}\ (r_A + r_O)]/9\ (r_B + r_O) \quad [5]$$

Using for r_B average ionic radii of M(III) and Li(I) (r(Li) = 66 pm), one obtains $t \cong 1.027$ for the solids in Table 9 besides $La_2Li_{1/2}Au_{1/2}O_4$, and $t \cong 1.004$ for the latter compound. Presumably, both factors—the geometrical cause and the increased vibronic coupling of Au(III) compared to Cu(III)—seem to stabilize the ordered Nd_2CuO_4 structure in the case of Au(III).

Concluding, we state that the available structural and spectroscopic evidence indicates that the compounds $La_2Li_{1/2}M_{1/2}O_4$ with M(III) = Co, Ni, and Cu crystallize in a superstructure of the K_2NiF_4 lattice with an ordered cation distribution between Li(I) and M(III) on the octahedral sites and with all M(III) cations in the low-spin configuration. Very probably the solids with Al(III), Ga(III), and Mn(III) possess the same structure.

ACKNOWLEDGMENT

We are grateful to Dr. A. Möller (University of Köln) for performing magnetic measurements of the Ni(III) compound.

REFERENCES

1. D. Balz and K. Plieth, *Z. Elektrochem.* **59,** 545 (1955).
2. G. Blasse, *J. Inorg. Nucl. Chem.* **27,** 2683 (1965).
3. G. Demazeau, C. Parent, M. Pouchard, and P. Hagenmüller, *Mater. Res. Bull.* **7,** 913 (1972).
4. G. Demazeau, M. Pouchard, M. Thomas, J. F. Colombet, J. C. Grenier, L. Fournès, J. L. Soubeyroux, and P. Hagenmüller, *Mater. Res. Bull.* **15,** 451 (1980).
5. G. Demazeau, J. L. Marty, M. Pouchard, Th. Rojo, J. M. Dance, and P. Hagenmüller, *Mater. Res. Bull.* **16,** 47 (1981).
6. R. H. Mohan Ram, K. K. Singh, W. H. Madhusudan, P. Ganguly, and C. N. R. Rao, *Mater. Res. Bull.* **18,** 703 (1983).
7. B. Buffat, G. Demazeau, M. Pouchard, J. M. Dance, and P. Hagenmüller, *J. Solid State Chem.* **50,** 33 (1983).
8. G. Demazeau, B. Buffat, M. Pouchard, and P. Hagenmüller, *J. Solid StateChem.* **54,** 389 (1984).
9. W. Pietzuch, S. A. Warda, W. Massa, and D. Reinen, unpublished results.
10. F. Abbatista, M. Vallino, and D. Mazza, *Inorg. Chim. Acta* **140,** 147 (1987).
11. D. Belder, Diploma Thesis, Marburg, 1991.
12. F. Abbatista and M. Vallino, *Atti Accad. Sci. Torino* **116,** 89 (1982).
13. K. Harms and W. Massa, LCORR, Programm zur Korrektur des $\lambda/2$-Effekts anRöntgenbeugungsdaten, Marburg, 1996.
14. G. M. Sheldrick, SHELXL-93, Program for the Refinement of Crystal Structures, University of Göttingen, Germany, 1993.
15. G. M. Sheldrick, SHELXL-96, Program for the Refinement of Crystal Structures, Beta Test Version 3.0. University of Göttingen, Germany, 1996.
16. "International Tables for Crystallography" (A. J. C. Wilson, Ed.), Vol. C. Kluwer Academic Publishers, Dordrecht, 1992.
17. SHELXTL, Release 5.05, Siemens Analytical X-ray Instruments Inc., Madison, WI, 1996.
18. F. Hahn and W. Massa, TWINXL, Program zur Aufbereitung von Datensätzen verzwillingter Kristalle, Marburg, 1996.
19. R. D. Shannon, *Acta Crystallogr., Sect. A* **32,** 751 (1976).
20. D. Reinen and C. Friebel, *Struct. Bonding* **37,** 1 (1979).
21. D. I. Khomskii and K. I. Kugel, *Solid State Commun.* **13,** 763 (1973); C. Friebel and D. Reinen, *Z. Anorg. Allg. Chem.* **407,** 193 (1974); D. Reinen and S. Krause, *Inorg. Chem.* **20,** 2750 (1981).
22. M. Hidaka, K. Inoue, I. Yamada, and P. J. Walker, *Physica B* **121,** 343 (1983).
23. K. Hestermann and R. Hoppe, *Z. Anorg. Allg. Chem.* **367,** 249, and 261 (1969).
24. V. Adelsköld, L. Eriksson, P. L. Wang, and P. E. Werner, *Acta Crystallogr., Sect. C* **44,** 597(1988).
25. H. K. Müller-Buschbaum and W. Wollschläger, *Z. Anorg. Allg. Chem.* **414,** 76 (1975).
26. S. A. Warda, W. Massa, D. Reinen, Z. Hu, and G. Kainde, *J. Solid State Chem.*, to be submitted.
27. D. Reinen, *Struct. Bonding* **6,** 30 (1969).
28. G. C. Allen and K. D. Warren, *Struct. Bonding* **9,** 49 (1971).
29. D. Reinen, C. Friebel, and V. Propach, *Z. Anorg. Allg. Chem.* **408,** 187 (1974).
30. C. K. Jørgensen, "Oxidation Numbers and Oxidation States," Springer, Berlin, Heidelberg, New York, 1969.
31. D. Reinen, *Theoret. Chim. Acta* **5,** 312 (1966).
32. D. Reinen, U. Kesper, and D. Belder, *J. Solid State Chem.* **116,** 355 (1995).
33. D. Reinen, M. Atanasov, G. St. Nikolov, and F. Steffens, *Inorg. Chem.* **27,** 1678(1988).
34. D. Reinen and J. Wegwerth, *Physica C* **183,** 261 (1991).
35. D. D. Samra, O. Strebel, C. T. Simmons, U. Neukirch, G. Kaindl, R. Hoppe, andH.P. Müller, *Phys. Rev. B* **37,** 9784 (1988).
36. M. Atanasov and D. Reinen, *J. Electron Spectrosc. Relat. Phenom.* **86,** 185 (1997).
37. Z. Hu, G. Kaindl, S. A. Warda, D. Reinen, F. M. F. de Groot, and B. G. Müller, *Chem. Phys.*, in press (1998).
38. P. Köhler, W. Massa, D. Reinen, B. Hofmann, and R. Hoppe, *Z. Anorg. Allg. Chem.* **446,** 131 (1978).
39. F. Abbatista, M. Vallino, and D. Mazza, *J. Less Common Met.* **110,** 391(1985).
40. B-H. Chen, *J. Solid State Chem.* **125,** 63 (1996).